Individual Tooth Segmentation in Two Dimensional Human Teeth Image

Seongeun Kim

Department of Mathematical Sciences, KAIST, Daejeon 34141, Korea

Abstract

In this paper, we propose a segmentation method.

Key words Image Processing, Neural Networks, Data Processing
AMS subject classifications 94A08, 68T07

1 Introduction

3차원 치아 복원의 필요성
- 전문적인 복원과정의 소모성
CT로부터 치아복원 연구들
파라노마 이미지로부터 복원 연구들
외부에서 촬영된 2차원 치아경계로부터 복원 가능 논문 [13]
연구의 목적

3.2에서 얻어낸 $\Omega \setminus \Omega_c$의 connected components의 컬렉션을 $\{\Omega_i\}_{i=1}^N$라고 하자. 각각의 연결요소들은 서로소이며, 경계는 그 자체로 active contour를 위한 initial contour가 될 수 있다. 즉, 각 i에 대하여, $\partial\Omega_i$를 zero level set으로 갖고, 영역에서 음수인 signed distance function $\phi_{i,\,0}$를 생각할 수 있으며 이 초기 컨투어로부터 정확한 edge를 검출하기 위해 proposed competing force $F_{c,i}$ in a level set formulation:

$$\begin{aligned} \frac{\partial}{\partial t}\phi_i(x,\,t) &= \mu\kappa(\phi_i)\,|\nabla\phi_i| + \chi_{\Omega\setminus\Omega_a} F_{c,\,i}\,|\nabla\phi_i| + \chi_{\Omega\setminus\Omega_a} - \chi_{\Omega_a} F_a\cdot\nabla\phi\,, \\ \phi_i(x,\,0) &= \phi_{i,\,0}\,, \end{aligned} \tag{1.1}$$

where F_a is the GADF in **??**, F_b is the SR force and .

2 Background

In this section, we briefly review geometric attraction-driven flow (GADF) [5] and edge region, which plays important role for segmenting individual tooth. We will derive how to obtain edge regions by concerning the problematic features of teeth image.

2.1 Geometric Attraction-Driven Flow

Assume there is a smooth gray image $I : \Omega \subset \mathbf{R}^2 \to [0,\,1]$. The image intensity changes rapidly on the boundary of two objects in the image. Thus, we define a point $x \in \Omega$ as an edge of the

image if

$$u_x''(0) = 0\,, \tag{2.1}$$

where

$$u_x(s) = I\left(x + s\frac{\nabla I(x)}{|\nabla I(x)|}\right)\,.$$

The GADF is defined as

$$F_a(x) = \mathrm{sgn}(\ell(x))\frac{\nabla I(x)}{|\nabla I(x)|}, \quad \forall x \in \Omega\,, \tag{2.2}$$

where the sgn is a sign function and

$$\ell(x) = \int_0^{\epsilon} u_x'(s)ds - \int_{-\epsilon}^{0} u_x'(s)ds \quad \text{for a small } \epsilon > 0\,,$$

By the definition, $F_a(x)$ directs the candidates of edges on the line $x + s\frac{\nabla I(x)}{|\nabla I(x)|}$ that is the points on which $u_x''(s) = 0$. An edge region means a region where an edge is thought to exist. In [5], edge region is defined by using regions where F_a are facing each other, i.e.

$$\Omega_a = \delta_{S_3}\left(\Omega_E\right)\,, \tag{2.3}$$

where δ_{S_3} is a dilation function using the 3×3 window S_3 and

$$\Omega_E = \{x \in \Omega \mid F_a(x^*) \cdot F_a(x) < 0 \text{ and } x^* = x + F_a(x)\}\,. \tag{2.4}$$

Under this setting, contour evolution using a level set formulation that the initial contour approaches the edge in Ω_a and goes outward in $\Omega_b = \Omega \setminus \Omega_a$ is proposed:

$$\begin{aligned} \frac{\partial}{\partial t}\phi(x,\,t) &= \alpha\kappa\,|\nabla\phi| - \chi_{\Omega_a}F_a \cdot \nabla\phi + \chi_{\Omega_b}F_b|\nabla\phi|\,, \\ \phi(x,\,0) &= \phi_0(x)\,, \end{aligned} \tag{2.5}$$

where α is a constant, κ is the curvature of level set functions ϕ and χ_A is a characteristic function on the set A.

The GADF is naturally expandable with color images. For a color image $I : \Omega \subset \mathbf{R}^2 \to [0,\,1]^3$, we can consider a nonlinear structure tensor $\mathbf{M}$ from a nonlinear diffusion

$$\begin{aligned} \frac{\partial \mathbf{M}(x,\,t)}{\partial t} &= \nabla \cdot \left(h\left(\sum_{i,\,j=1}^{2} |\nabla M_{ij}(x,\,t)|^2\right)\nabla \mathbf{M}(x,\,t)\right)\,, \\ \mathbf{M}(x,\,0) &= \sum_{k=1}^{3} \nabla I_k(x) I_k(x)^T\,, \end{aligned}$$

and the diffused tensor $\mathbf{M}$ preserves local features of the image I [8, 12, 2, 4]. We can count the eigenvector with respect to the maximum eigenvalue of $\mathbf{M}$ as a gradient and then the defining GADF on color images is tractable.

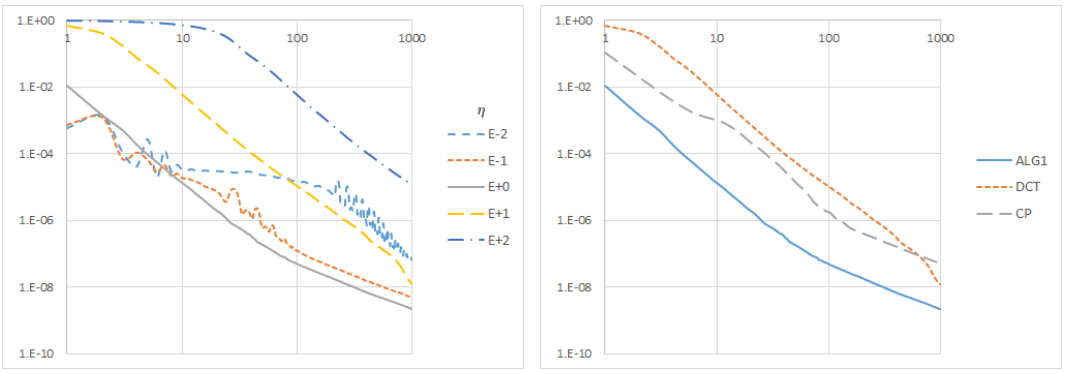

(a) (b)

Figure 1: (a) Human teeth image with weak edges

2.2 Weak edge detection

When the change of intensity at the edge of an image is smaller than the neighborhood, we call it a weak edge. For a gray image I,

$$\nabla|\nabla I| \parallel \mathcal{H}_x(I)\nabla I$$

is easily obtained from calculations, and it show that the direction of $\nabla|\nabla I|$ is getting differ to the ∇I whenever change of intensities is smaller than neighborhood, because of the affection of the hessian matrix $\mathcal{H}_x(I)$. In other words, around weak edges, it is difficult to determine the edge or edge region simply by using the color information. However, as can be seen in (2.2), GADF is defined to have one of the directions of ∇I and $-\nabla I$, and thus it is possible to find an edge region that includes all weak edges without regardless of the amount of intensity change. Weak edges are common in human teeth images. In particular, it appears at the boundary between the teeth and the gums and at the boundary between two teeth with similar color and brightness. Figure 1 shows the weak edges seen in the tooth image and the edges or edge regions detected by different methods.

2.3 Edge regions outside the tooth boundaries

In reality, teeth image contains various edges appear outside of the tooth boundary due to inhomogeneities of the object surface or noise present in the image. Because of these edges, the edge region calculated from GADF includes many connected regions outside the tooth boundary. These unnecessary regions prevent the contour from getting closed to the boundary of interest, so we have to handle them. These regions can be roughly divided into three categories according to the causes:

(1) Noise or small stains,

(2) Large and faded stains having some clear parts,

(3) Strong specular reflection.

The edge regions caused by (1) are small and the color of the image around them is relatively flat while edge regions caused by the tooth boundary are supposed to very large and colors are

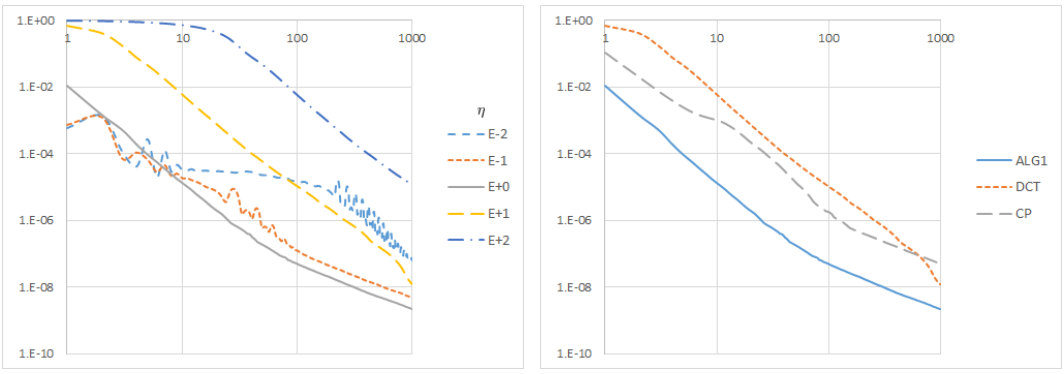

(a) (b)

Figure 2: (a) Human teeth image with weak edges

changed rapidly around them. Therefore, the regions caused by (1) can be removed preferentially. (2) Some stains on the image makes a relatively large edge region. It is not easy to distinguish these regions from edge regions at the tooth boundary only by size and color information. However, when the whole of the stain is not clear and there is some faded part, the end of the edge region in that part is exposed. As the initial contour evolves, if it meets the ends, it shrinks along the GADF and because of the curvature term of 2.5, so the edge regions arising from the stains can be canceled out. On the other hand, edge regions arisen from (3) are in large and closed shape. Because of the shape in which the ends are not exposed, it cannot be neutralized using the contour evolution, and it is impossible to distinguish between the edge regions caused from the tooth boundary using shape and color information. These edge regions block the path of the contour like a barrier and makes it difficult to find the correct tooth boundary, and as a result, they are being main obstacles of the individual tooth segmentation. These edge regions and contour evolution around them are appeared in Figure 2.

2.4 Avoidance of light reflections in the teeth image

There previous studies that tries to remove this light reflections of a single image [9, 14, 10, 3]. They attempts to separate an image with reflections into an image without reflections and reflections and for this, image intensity histogram is used or a dichromatic image model is assumed. This methods are basically to use color information of the reflective region but in the case of tooth images, due to the nature of the human teeth, the light reflection and the color of the tooth surface are almost the same. For this reason, when the existing methods are actually applied, a part of the tooth surface is also removed with light reflection. There have also been attempts to remove light reflection on teeth images by using the single layer perceptron [6], but which is limited in its application to a wide range of images as we are targeting.

Above all, even if light reflection is removed from the teeth image, individual tooth can be segmented immediately. If a lot of unnecessary edge regions are appeared since of the image condition or strong stains, then it is still difficult to segment individual tooth. Therefore we directly get only the edge region near the tooth boundary, regardless of any stains or noise in the image and for this, we use a supervised learning method of neural networks.

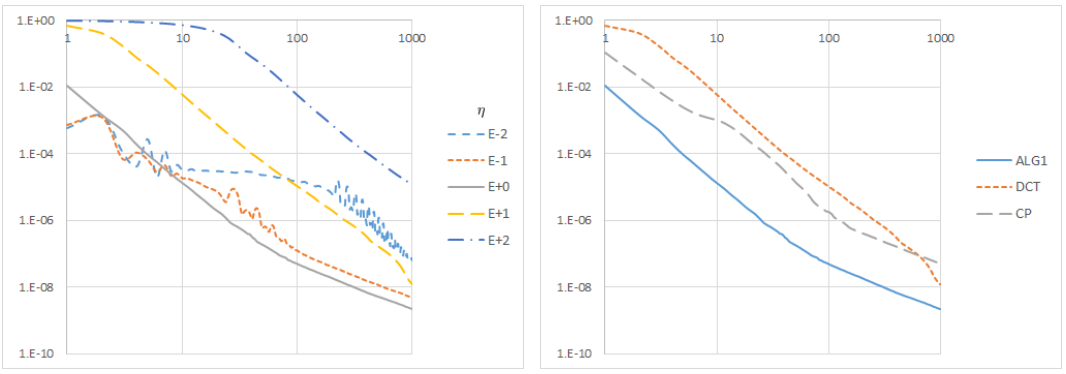

(a) (b)

Figure 3: Algorithm flowchart for the proposed method

3 Proposed Method

In this section, we describe the steps of the proposed individual tooth segmentation. It is done through the following three main steps, and the whole process is shown in Figure 3:

(1) Data labeling and training strategy,

(2) Obtaining an edge region candidate from a neural network and region trimming,

(3) Segmentation using active contours competing with each other.

3.1 Data labeling and training strategy

Labels for input data are indispensable for supervised learning. In general, labels do not accompany the data, and they should be create them by human force. However, this kind of human labeling has to pay too much time and effort, and also there is a big disadvantage that there is no guarantee that the label completely matches the information of the image. For example, we want to take the edge region on tooth boundary as label, and the edge region obtained from GADF is created around the point that exactly satisfies 2.1, whereas there is no such guarantee in the case of direct labeling by humans. Therefore, we devised a labeling method that reflects the information of the teeth image well while minimizing the human touch. First, regions only present on the tooth boundary are manually selected among the connected regions contained in Ω_E which is the region where GADF faces each other, we denotes the selected region Ω_S. After that, the label

$$\Omega_L = \delta_{S_\omega}(\Omega_S)$$

is obtained by dilation using a S_ω. This process can be viewed in (a), (b) and (c) of Figure 8.

In the labeling, we did only selection process to minimize human touch. Because of this simplicity, the label does not perfectly match the tooth boundaries, so the label contains many disconnects (called leakages) and unnecessary parts. The unnecessary parts are actually not related to the tooth boundary but selected because they are connected to them. See Figure 8.

In general, the labels that are considered perfectly fit to the data are used for training. Therefore, well-known image-to-image networks [7, 11] have connections to preserve information

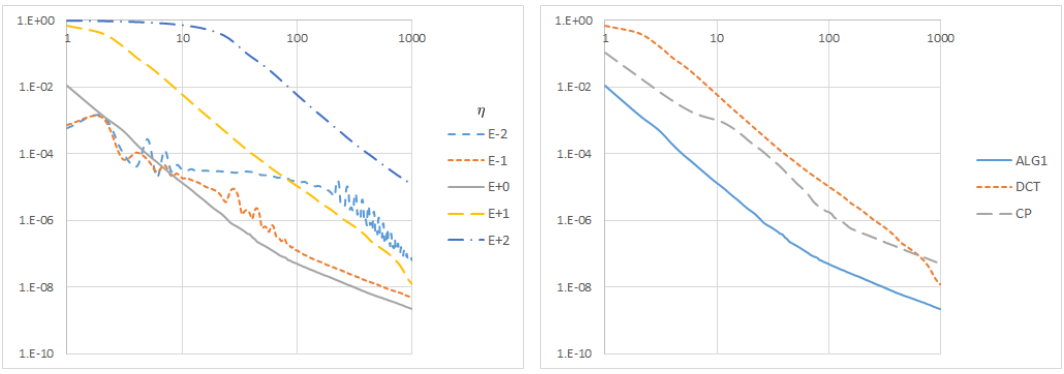

(a) (b)

Figure 4: Algorithm flowchart for the proposed method

at high resolution in order to perfectly keep even the smallest details of a label. However, since the detail in the label is corrupted, if we try to train to retain all the details in the label, we can predict that the result will also have corrupted detail. Therefore, to learn this label well, we used an encoder-decoder model with a much smaller latent variable compared to the input. The structure of the neural network that we use is appeared in Figure 4.

3.2 Obtaining an edge region candidate from a neural network and region trimming

The neural network obtained through training in 3.1 infers a probability map $\hat{Y} : \Omega \in \mathbf{R}^2 \to [0, 1]$ when it takes an image $I : \Omega \to [0, 1]$, and here $\hat{Y}(x)$ is the probability of having a tooth boundary at x. We call the region defined by

$$\Omega_c = \left\{ x \in \Omega \mid \hat{Y}(x) > \alpha \right\}$$

as an edge region candidate from the neural network. As shown in (b) of Figure 5, Ω_c is formed only at the boundary of the tooth, not the causes listed in 2.3. In particular, the label included the edge regions caused by light reflections connected to the tooth boundary without removing it, but Ω_c included the region only at the tooth boundary excluding all other regions. On the other hand, Ω_c is not yet perfect. Since it contains small fragments and leakages, apply a trimming process to Ω_c to form closed individual tooth regions. First, small fragments and holes can be easily removed and filled in compared to the size of Ω. Then it remains to plug the leakages, which requires first figuring out where the leakages occurs. We assume that the leakages definitely consist of more than one end. Thus, finding the ends at Ω_c and extending them to fill the leakage is what we are trying to do. Since Ω_c is a region obtained by thresholding the probability map, the thickness and shape of the region are not uniform, and so it is not easy to mathematically define the end. Furthermore, in order to determine which direction to extend the region at the end, the direction in which the region travels must be obtained, but it is not easy to find the direction directly from Ω_c. By investigating to 8-pixel connected topological skeleton [1], we were able to solve the problem. In the Figure 6 shows ends and curves obtained from the skeleton. More details are present in the Appendix A.

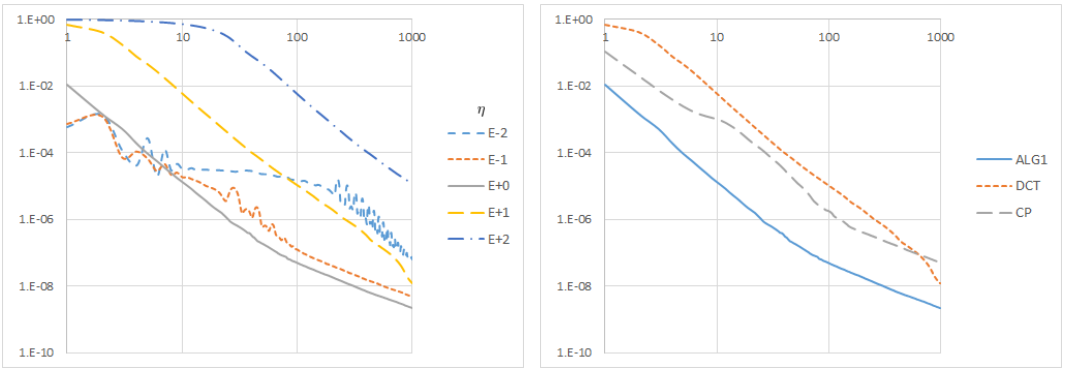

(a) (b)

Figure 5: Algorithm flowchart for the proposed method

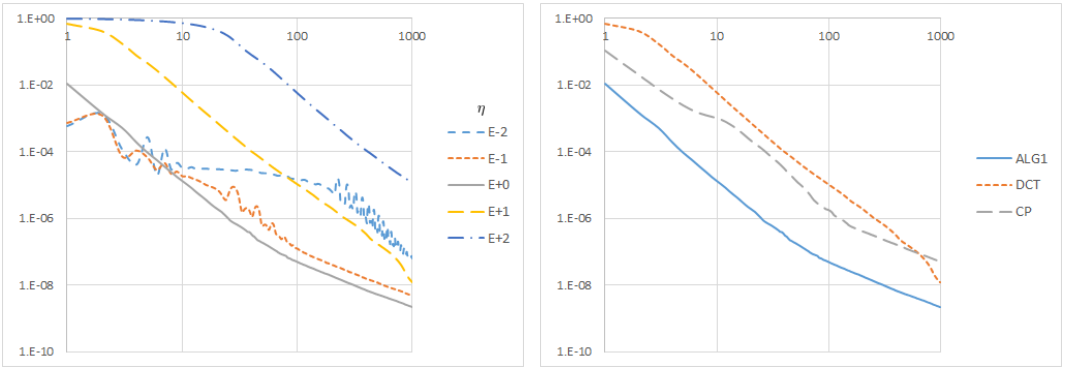

(a) (b)

Figure 6: Algorithm flowchart for the proposed method

3.3 Segmentation using balloon shaped competing force

Let $\{\Omega_i\}_{i=1}^n$ be a collection of disjoint subsets of a given domain $\Omega \subset \mathbf{R}^2$. For a purpose of finding edge, we evolves contour C_i^t which is initially the boundaries of $\{\Omega_i\}_{i=1}^n$, i.e. $C_i^0 = \partial\Omega_i$ for $i = 1, \cdots, n$. Suppose that there are no edge information, then we are going to decide the edge by competing on the boundaries to other regions. For this, we design a balloon shaped inflating force competing on the interfaces using level set formulation. Let $\phi_{i,\,0}$ be a signed distance function which is zero on $\partial\Omega_i$ and negative in Ω_i, then $F_{c,\,i}$ is defined as:

$$F_{c,\,i}(x,\,t) = \begin{cases} -1 & \text{if} \quad \phi_i(x,\,t) < 0, \\ s\left(1 - \sum_{j \neq i} \phi_j(x,\,t)\right) & \text{otherwise,} \end{cases}$$

where s is a function which roles as the identity on positive and 0 on negative. Observe that in the level set formulation:

$$\begin{aligned} \frac{\partial}{\partial t}\phi_i(x,\,t) &= \mu\kappa(\phi_i)\,|\nabla\phi_i| + F_{c,\,i}\,|\nabla\phi_i|\,, \\ \phi_i(x,\,0) &= \phi_{i,\,0}\,, \end{aligned}$$

$F_{c,\,i}$ pushes C_i outward and when it faces another contour, $F_{c,\,i}$ let them decide edge line without invade each other. The shape of boundary can be adjusted by the coefficient of the curvature term. Larger μ gives more forces to make the boundary flat. In (a) and (b) of Figure 7, the evolution processes for several initials are shown. Furthermore, suppose that we have some barrier regions $\mathcal{B} \in \Omega$ defined where the contours are obstructed and cannot be crossed. Then we can consider a level set formulation:

$$\begin{aligned} \frac{\partial}{\partial t}\phi_i(x,\,t) &= \mu\kappa(\phi_i)\,|\nabla\phi_i| + \chi_{\mathcal{B}}F_{c,\,i}\,|\nabla\phi_i|\,, \\ \phi_i(x,\,0) &= \phi_{i,\,0}\,, \end{aligned}$$

which works only outside of $\mathcal{B}$. In (c) and (d) of Figure 7, a simple example is there.

For the region obtained from 3.2, we can assume that there are no edge outside the region Ω_c. Following the level set evolution made from (1.1), the initial contours are proceeds outward, respectively and when it enters into Ω_a and Ω_c, then edge is determined by GADF and F_v, respectively. On the other side, if neither there are no Ω_a nor edge is not decided by F_v, then the contour faces other contour and edge will be decided by competition between them.

3.4 Teeth and non-teeth region classification

As a final step, classification of the segmented regions is remained. Since our goal is to segment an individual tooth, we are going to classify a teeth and a non-tooth regions among the segmented regions, and take only the tooth regions. In the human teeth image, teeth and non-tooth regions can be distinguished in terms of morphological and color information. First, while tooth have a convex-like shape, the non-tooth region has a lot of curves on its boundary due to the shape of the roots of the teeth. Therefore, by considering the criterion $C_m < 0$ it is possible to classify regions with too many curvatures on the boundary where

$$C_m = \int_{\{\phi=0\}} \nabla \cdot \frac{\nabla\phi}{|\nabla\phi|}\,dx\,, \tag{3.1}$$

and ϕ is a SDF negative in and zero on the boundary of the region, respectively.

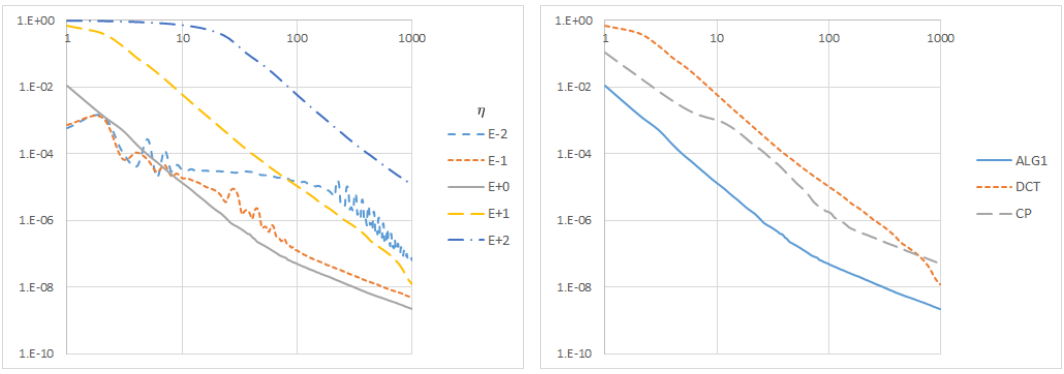

(a) (b)

Figure 7: Algorithm flowchart for the proposed method

On the other hand, there is another very obvious feature of human teeth, which is that the teeth are consist of (at most) two rows, the upper and the lower jaws. Paying attention to this point, we first drew a vertical lines in each segmented region, and mark the region if there are more regions than the number of teeth row. Then, by analyzing the colors on the vertical line, the tooth and non-tooth regions can be divided. This idea is very simple but powerful. Teeth image has inhomogeneities of luminance because the human teeth are curved inward. Thus it is very hard to classify teeth and non-tooth region by using the colors of image directly. But, each vertical line can be considered as curved inward by the same amount, and in fact, classification using colors on the line gives a way better result. In practice, more elaborate works are done than written here and details are provided in the Appendix B.

In summary, the region classification yeld two steps: (1) (3.1) at the boundary of the regions is calculated, and the region with $C_m < 0$ is classified as a non-tooth region. (2) The remaining region were classified based on the number of regions and color information on the vertical line.

4 Experimental results and numerical aspect

The explicit Euler scheme is used for time discretization of (1.1).

5 Conclusion

A Finding edges and extension from the edge

A.1 An 8-connected topological skelton

The topological skeleton $\mathcal{S}$ of Ω_c can be defined in various ways that are equivalent to each other. In this paper, we use the ridge of a signed distance function:

$$\mathcal{S} = \{x \in \Omega_c \mid |\nabla\phi(x)| = 0\} \ ,$$

where $\phi = \mathrm{SDF}(\Omega_c)$. This can be discretized in a natural way, and let $\mathcal{S}_{\Omega_c}$ denote it. Now consider the set of all subsets of $\mathcal{S}_{\Omega_c}$ whose 8-connectivities are coincide. Then we can find a maximal $\mathcal{S}^8_{\Omega_c} \subset \mathcal{S}_{\Omega_c}$ in the set such that $\forall x \in \mathcal{S}^8_{\Omega_c}$ are in only one of the two categories: (1) the connectivity

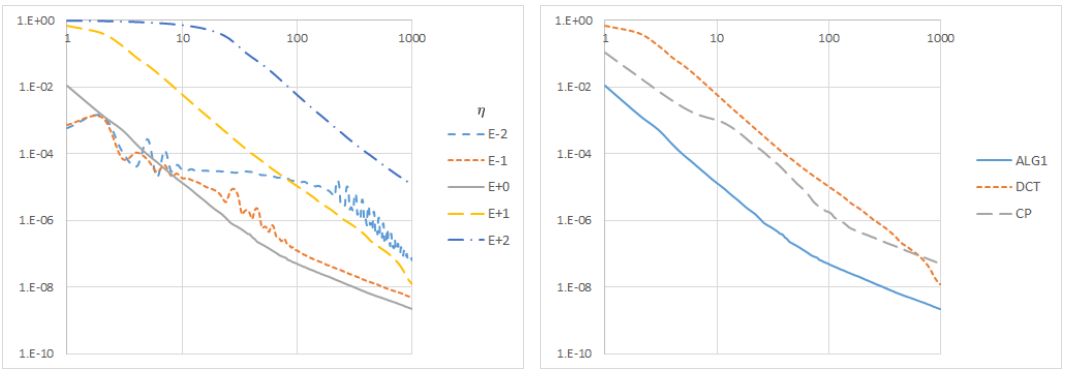

(a) (b)

Figure 8: Algorithm flowchart for the proposed method

of $\mathcal{S}^8_{\Omega_c}$ is changed if x is removed or (2) x is an end of $\mathcal{S}^8_{\Omega_c}$. Look at the Figure 9. Here, we define a point x of a skeleton as an end if 3×3 window centered at x is the same as one of Figure 9. Observe that in a 3×3 window of an end point of $\mathcal{S}^8_{\Omega_c}$, there are only two points end point itself and the other point. Let the end point be x_0 and let the other point be x_1. Next, in the x_1, there may be several points x_0, x_1 and the others. Let the set of other points be $p(x_1)$. A parametric curve $\lambda : \mathbf{Z} \cup [0,\, L] \to \Omega$ can be obtained by the Algorithm 1.

Algorithm 1 Algorithm for obtaining the representative curve for $\mathcal{S}^8_{\Omega_c}$

Choose $L \in \mathbf{Z}_{>0}$. Let $n = 0$, $x_0 \in E(\mathcal{S}^8_{\Omega_c})$ and $x_1 \in p(x_0)$.
while $p_x^{(n)} == 1$ or $|\lambda| < L$
$p_x^{(n)} = p(p_x^{(n-1)})$
end while

A.2 Extension from ends

Using $\gamma(t)$, we can calculate tangent and curvature at the end point and from now, we regard the ends, tangents and curvatures as of the region Ω_c. We plan to fill the leakages by trying to extend it sequentially in a more plausible direction. The basic strategy in this process is to return to the end before the extension if the leakage is not closed after a certain length of extension, and after that, start extension in the next direction. This is because we do not want to complicate the region by extensions that cannot reached, and it is assume that if the direction is appropriate, then the ends should be able to close the leakages with even a small extension. For the extension, three different cases are considered:

(1) Using Ω_a coincident with the direction of the end.
Suppose that Ω_c continued along an edge of an image and breaks, resulting in a leakage. If the edge is still continued even in the leakage, then Ω_a should exist with the same direction as Ω_c. Therefore, we extend $E(\Omega_c)$ along Ω_a when the directions of Ω_a and Ω_c are similar at the $E(\Omega_c)$, i.e.,

$$|T(e) \cdot F_a(e)| < \frac{1}{2}, \quad e \in E(\mathcal{S}^8_{\Omega_c}).$$

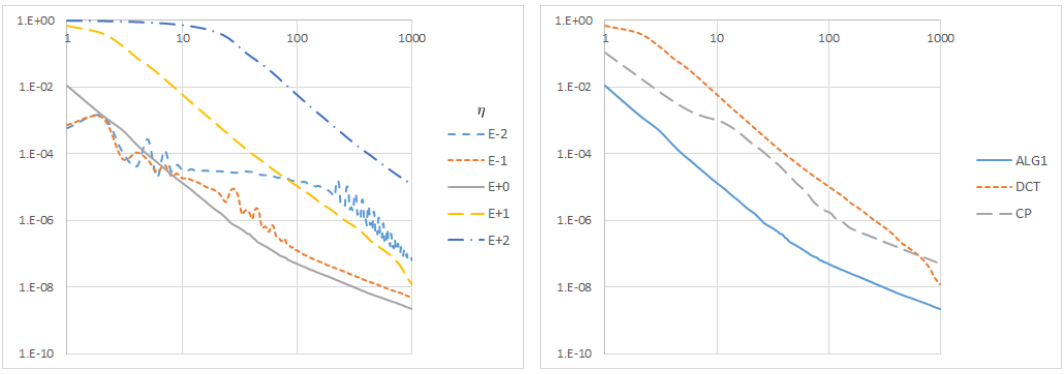

(a) (b)

Figure 9: Algorithm flowchart for the proposed method

(2) Using quadratic curve.
When there are no Ω_a with the direction at the end, then we extend the end following the quadratic curve which is the best approximation of $\gamma(t)$ in a least square sense.

(3) Using straight line.
Of the remaining leakages, those that can be filled with a small extension are simply extended in a straight line.

B Region classification using vertical lines

Suppose that a domain Ω of a teeth image I is partitioned by the 3.3. Let x is a point in a member of partition of Ω and let $V(x)$ be a vertical line through the point x. Since human teeth have only two teeth, upper and lower, it can be assumed that non-tooth regions exist only when there are three or more regions through which $V(x)$ passes, and let those regions be $\{\Omega_i\}_{i=1}^{N}$. We try to classify these regions as whether they are teeth or not using color information. However, since human teeth are curved, the distance between the camera and each tooth is not constant even in one image. Since the brightness and color of the image vary according to the degree of curved from the front, classification through color information for the entire region cannot be easily achieved. In this circumstance, we can assume that the teeth below the line curve to a similar degree from the front, so it makes sense to analyze the colors at $V(x)$ and classify the regions thought $V(x)$. In general, human teeth and neighbor parts are usually considered as white and red, respectively but teeth contain a lot more yellow than expected, which is due to contaminants on the tooth surface. Thus we moved from RGB space to CIELAB [15] color space to effectively separate the three colors, white, red and yellow. Let us denote the image represented to CIELAB as $I_{LAB} = (I_L, I_a, I_b)$. Here the k-means clustering algorithm is used. The important parameter for the k-means algorithm is setting initial seeds on which the algorithm start clustering. We set a total of three initial points, each to start close to white teeth, yellow teeth, and the other relatively red parts. The detailed initial points p_1, p_2, p_3 are as follows:

$$
\begin{aligned}
p_1 &= (100, 0, 0)\,, \\
p_2 &= I_{LAB}(a^*)\,, \\
p_3 &= (50,\ 0,\ \max(I_b))\,,
\end{aligned}
$$

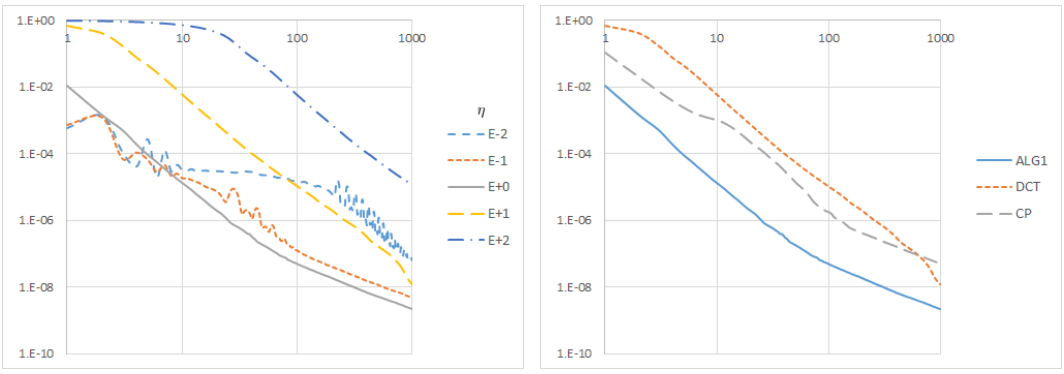

(a) (b)

Figure 10: Algorithm flowchart for the proposed method

where $a^* = \text{argmax} I_a$. In practice, there are 50% of points are used for each member of partition of Ω and class of the member is determined by the votes of each point. The classification process using vertical lines is shown in Figure 10.

References

[1] H. Blum et al., *A transformation for extracting new descriptors of shape*, vol. 43, MIT press Cambridge, MA, 1967.

[2] T. Brox, J. Weickert, B. Burgeth, and P. Mrázek, *Nonlinear structure tensors*, Image and Vision Computing, 24 (2006), pp. 41–55.

[3] J. Guo, Z. Zhou, and L. Wang, *Single image highlight removal with a sparse and low-rank reflection model*, in Proceedings of the European Conference on Computer Vision (ECCV), September 2018.

[4] J. Hahn and C.-O. Lee, *A nonlinear structure tensor with the diffusivity matrix composed of the image gradient*, Journal of Mathematical Imaging and Vision, 34 (2009), pp. 137–151.

[5] J. Hahn and C.-O. Lee, *Geometric attraction-driven flow for image segmentation and boundary detection*, Journal of Visual Communication and Image Representation, 21 (2010), pp. 56–66.

[6] S.-T. Lee, T.-H. Yoon, K.-S. Kim, K.-D. Kim, and W. Park, *Removal of specular reflections in tooth color image by perceptron neural nets*, in 2010 2nd International Conference on Signal Processing Systems, vol. 1, IEEE, 2010, pp. V1–285.

[7] O. Ronneberger, P. Fischer, and T. Brox, *U-net: Convolutional networks for biomedical image segmentation*, in International Conference on Medical image computing and computer-assisted intervention, Springer, 2015, pp. 234–241.

[8] M. Rousson, T. Brox, and R. Deriche, *Active unsupervised texture segmentation on a diffusion based feature space*, in 2003 IEEE Computer Society Conference on Computer Vision and Pattern Recognition, 2003. Proceedings., vol. 2, IEEE, 2003, pp. II–699.

[9] T. H. Stehle, *Specular reflection removal in endoscopic images*, in Proceedings of the 10th international student conference on electrical engineering, Citeseer, 2006.

[10] J. Suo, D. An, X. Ji, H. Wang, and Q. Dai, *Fast and high quality highlight removal from a single image*, IEEE Transactions on Image Processing, 25 (2016), pp. 5441–5454.

[11] J. Wang, K. Sun, T. Cheng, B. Jiang, C. Deng, Y. Zhao, D. Liu, Y. Mu, M. Tan, X. Wang, W. Liu, and B. Xiao, *Deep high-resolution representation learning for visual recognition*, 2020.

[12] J. Weickert, *Coherence-enhancing diffusion filtering*, International Journal of Computer Vision, 31 (2004), pp. 111–127.

[13] C. Wu, D. Bradley, P. Garrido, M. Zollhöfer, C. Theobalt, M. Gross, and T. Beeler, *Model-Based Teeth Reconstruction*, ACM Transactions on Graphics (TOG), 35 (2016).

[14] Q. Yang, J. Tang, and N. Ahuja, *Efficient and robust specular highlight removal*, IEEE Transactions on Pattern Analysis and Machine Intelligence, 37 (2015), pp. 1304–1311.

[15] A. Zeileis, K. Hornik, and P. Murrell, *Escaping rgbland: Selecting colors for statistical graphics*, Computational Statistics and Data Analysis, 53 (2009), pp. 3259–3270.